Infrared Thermography of Cavitation Thermal Effects in Water

Aljaž Osterman[*] - Matevž Dular - Marko Hočevar - Brane Širok
Faculty of Mechanical Engineering, University of Ljubljana, Slovenia

Although the thermal effects of cavitation are believed to be negligible for cavitation in water, they were successfully experimentally measured using infrared thermography. Cavitation was generated in a small container holding about 500 ml of water. It was oscillated with ultrasonic frequencies of 42 kHz to trigger growth and collapse of bubbles. For the temperature measurements a high-speed thermovision camera was used. It captures light in infrared spectrum with wavelength of 3-5 μm. The frequency of temperature field acquisition was set to 600 Hz. A silicon glass, which is transparent in the infrared light spectrum, was attached to a cylinder and partially submerged into water. Bubbles, which tend to appear in the vicinity of solid surface, appeared on the submerged side of the glass. The visual path for the thermovision camera was: air – silicon glass – water. In this way, the temperatures on the submerged side of the silicon glass where bubble growth and implosions occur could be measured. With the applied thermographic method small but distinctive local decreases of temperature (with magnitudes up to 0.3 K), caused by cavitation, were detected.
Keywords: cavitation, ultrasound, temperature, IR thermography, bubbles

0 INTRODUCTION

Cavitation phenomenon, characterized by vapor generation and condensation, frequently occurs in industrial fluid flows. Often it is accompanied by effects like vibration, increase of hydrodynamic drag, changes in the flow hydrodynamics, noise, erosion, light effects such as sonoluminescence as well as thermal effects. They are often neglected since cavitation is, generally speaking (on a large scale), an isothermal phenomenon [1]. However, on a small scale (a single bubble), significant thermal effects such as a considerably high rise in temperature when the bubble collapses and local cooling of the bubble surrounding at its growth, take place. These phenomena are almost always in equilibrium (if energy for cavitation erosion, sonoluminiscence etc. is neglected). This means that the increase of the temperature must be balanced by its prior or later decrease. In this way, a quasi-isothermal nature of the cavitation is preserved.

As the pressure is locally decreased, conditions for evaporation (growth of the cavitation bubble) become plausible. To initiate the growth of cavitation bubble another condition is required: the presence of a cavitation nucleus in the region, represented by gas (air), trapped gas in wall fissures or dissolved in the fluid. From the incipient cavitation on, the nuclei are produced also by the bubble collapses. When both conditions are fulfilled, the bubble begins to grow and latent heat is sucked from the surrounding liquid, creating a thermal boundary layer. The result is a small local decrease of liquid temperature that is usually called "thermal delay" [1]. This temperature drop due to cavitation growth results in lower vapor pressure and is retarding cavitation growth because greater pressure drop is needed.

After the bubble reaches its maximum size, it collapses – the temperature (and also pressure) inside it increases very rapidly and reaches extreme values (e.g. 6700 K and 848 bar [2]).

Thermal delay can usually be neglected when dealing with fluids for which critical point temperature is much higher than the working temperature. In that case, heat gained during the bubble collapse is in quasi-equilibrium with the heat used for the bubble growth and the isothermal condition is fulfilled. In this case of equilibrium, the data from the study of thermal delay could be used for determining the conditions in the bubble at its collapse. On the other hand, the thermal delay becomes significant when the critical point temperature and fluid

---

*Corr. Author's Address: Faculty of Mechanical Engineering, Aškerčeva 6, SI – 1000 Ljubljana, Slovenia
aljaz.osterman@fs.uni-lj.si

working temperature lie close together (for example, in the case of cryogenic fluids [3]).

Cavitation can be generated by subjecting a liquid to an oscillating pressure field of a particular (usually ultrasonic) frequency. The local decreases and increases of pressure are caused by the inability of a fluid (due to inertia) to follow the oscillations of a solid wall. If the amplitude and the frequency of oscillations are adequate and a cavitation nucleus is present in the region, a bubble will appear and collapse in such a region. Therefore, on one hand it is a very fast phenomenon while on the other, it happens on a very small spatial scale.

Bearing in mind such a specific nature of cavitation, it is clear that an experimental approach on a local level is very difficult and not many experimental methods are available. For all types of cavitation it is also important that it reflects certain conditions of the flow so that the experimental method used does not alter the flow. Therefore, it is understandable that only few experimental data of cavitation thermal effects are available. This applies especially to the temperature measurements [4] and [5]. Some estimations of the influence of the thermal effect were done by comparing cavitation structures, based on visualization and pressure measurements [6] to [8].

In this paper a new experimental approach to cavitation is presented. A non-contact and non-invasive thermographic method was used to measure cavitation-dependent temperature fields. Temperature fields were measured because temperature plays such an important role in cavitation.

Measured cavitation thermal effects were in form of local appearance of colder areas. They were connected to thermal delay but due to the difference between temporal scales of the observed phenomena and a collapse time of a single cavitation bubble [1], a reconstruction of the bubble collapse was not possible.

Cavitation was generated in water using an ultrasonic cleaning device with an aim to bridge the gap between a common isothermal approach on a system scale and extreme local thermal phenomena driven by collapses. The aim was also to use the ultrasonic cleaning device as an example of how some cavitation effects have been favorably exploited. It is believed that the introduction of the thermographic method for

cavitation measurement and the obtained results can contribute to a better understanding of the cavitation phenomenon, thus improving many practical applications where cavitation is used [9].

1 EXPERIMENTAL SET UP

The experiment was performed under atmospheric pressure (approximately 1 bar) and the water temperature was close to the ambient (23°C). The whole experimental set-up is presented in Fig. 1.
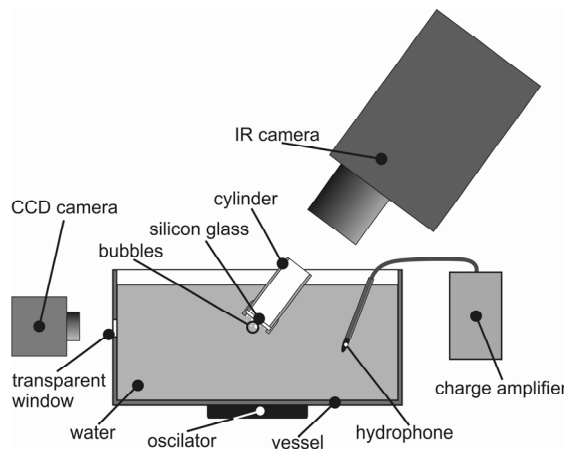

Fig. 1. *Experimental set-up*

A small vessel made out of stainless steel with a capacity of approximately 500 ml (dimensions are $140 \times 70 \times 60$ mm) was used. Beneath it an oscilator that produced periodic oscillations at a frequency of about 42 kHz, was mounted.

The ultrasonic frequency, causing water tank oscillations, was verified by measurements with the capacitive hydrophone Bruël & Kjær type 8103. Hydrophone was connected to the charge amplifier B&K type 2635. Data were sampled to a PC at 100 kHz which was below the upper frequency limits for the hydrophone (180 kHz) and the charge amplifier (200 kHz).

Measurements have been taken during the several hours of operation and in that period short sequences of data were recorded. It was confirmed that the main frequency, causing the cavitation phenomena, was 42 kHz, to which a network frequency of 50 Hz was added. As can be seen in Fig. 3, the spectral power of the 42 kHz signal was significantly higher than that of

Osterman, A. – Dular, M. – Hočevar, M. – Širok, B.

the 50 Hz signal. This means that the latter practically did not influence the results.

For an acquisition of the temperature field a high-speed thermovision camera CMT384SM - Thermosensorik was used. Its sensitive wavelength range lies between 3 and 5 µm. Temperature fields were taken at the water – observation window interface because in the measured spectrum water is not transparent to IR [10], while for the observation window IR transparent silicon with antireflective (AR) coating was used [11].

The acquisition frequency of the camera was set to 600 frames per second where the best results (in respect to the highest contrast and the lowest noise) were achieved. Frame size was 128 × 128 pixels and the integration time was 500 µs. The thermocamera had constant focal length and a pixel size of 55 µm was determined from a known geometry.

The high-speed thermovision camera was calibrated in the environment as used for the experiment. The constraint was constant and uniform temperature distribution which was achieved by mixing during long periods of time allowed for the system to reach certain temperature ranges at which the camera was calibrated. In this way, at each calibration temperature a referential temperature field was measured. Uncertainty of mean water operating temperature was conditional on the measurements with A-class Pt100 sensor and was ±0.2 K. However, our main goal was to quantify relative differences in non-uniform time-dependant temperature field. For a single element on the temperature sensor of the thermocamera (representing one pixel) the uncertainty of temperature changes relative to the operating temperature was only ±0.03 K.

A round silicon window 25 mm in diameter and 1 mm thick was used. The glass was coated to additionally ensure the desired absorption and reflection properties. The transmission of infrared radiation through the glass was measured and it was confirmed that the loss is minimal. It was attached to a cylinder and partially submerged into water. Bubbles, which tend to appear near the solid surface, appeared on the submerged side of the glass.

The visual path for the IR camera was: air – silicon glass – water-glass interface. This way the temperatures on the submerged (wetted) side

of the silicon glass, where bubbles grow and implode, could be measured. Due to its high absorption, the water itself is not transparent in the wavelength range between 3 to 5 µm – this was experimentally verified as 20 µm thick film of water let trough no IR light.

In a visible spectrum observations through a glass window in a side wall of the ultrasonic cleaning device were done with high-speed CCD camera MotionBLITZ Cube (Mikrotron GmbH). Acquisition rate was 1000 fps for a frame size of 1024 × 1280 pixels. The focus of the camera was on the lower (wetted) surface of the AR coated silicon window. The purpose was to monitor the appearance and behavior of bubbles in a region near the interface observed by the thermocamera.

2 RESULTS AND DISCUSSION

A strong tendency of bubbles to grow and collapse in the regions with an uneven surface and sharp edges was found (for example, at the contact point between the silicon window and the seal of the cylinder). This was expected since rough and uneven surfaces act as a cavitation nuclei generators, which stimulate bubble growth. Bubbles also appeared in the central part of the IR observation window, but they were quite dispersed. It is expected that for bubbles so distant (as shown in Fig. 2), their mutual interaction is very weak. In this view, the greatest effect on a collapse of the cavitation bubble is expected because of the presence of a solid wall, so that an impinging microjet forms [12] to [14].
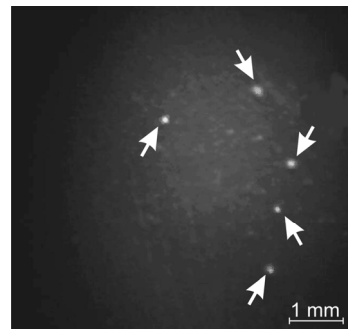

Fig. 2. *Conventional image of several cavitation bubbles on the silicon glass*

From the images in the visible spectrum also a size of the bubbles was estimated. The average size was 0.084 mm. The agreement between the observed size and a theoretically

predicted size was 93%. The difference is mostly due to visualization where the exact size of moving bubbles was difficult to determine. The theoretical size is a size of a bubble that has the same eigenfrequency as is the frequency of the ultrasound we used. A detailed relation is described with the following Eq. [15]:

$$f_{eig} = \frac{1}{2\pi}\sqrt{\frac{3n(p_\infty - p_v)}{\rho_l R^2} + \frac{2(3n-1)S}{\rho_l R^3} - \frac{8v_l^2}{R^4}}, \quad (1)$$

where f_{eig} is eigenfrequency of the bubble, n polytrophic constant, p_v vapor pressure, p_∞ referential pressure, R bubble radius, S surface tension, v_l kinematic viscosity of a liquid and ρ_l liquid density. For example, for water at 20 °C and frequency of 42 kHz the bubble radius is 0.078 mm.

The frequency of the ultrasound was obtained from hydrophone measurements of pressure oscillations in water during the ultrasonic cleaning device operation. From a time signal a frequency spectrum was obtained by using discrete Fourier transformation. The spectrum is presented in Fig. 3, in which a distinctive peak that lies at 42 kHz can be identified (Nyquist frequency is 50 kHz).
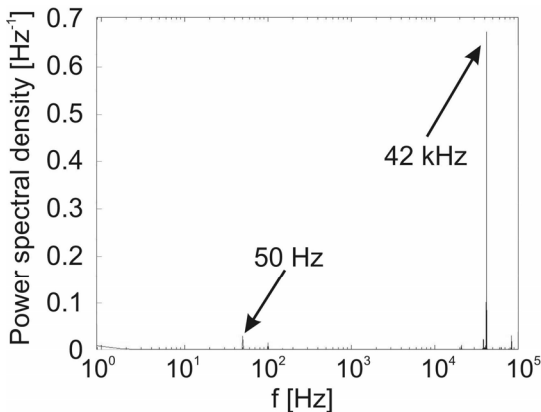

Fig. 3. *Frequency spectrum from hydrophone measurements*

2.1 Temperature Fields from IR Measurements

With the thermocamera the temperature fields of the water-silicon window interface were measured and some distinctive phenomena of temperature changes related to cavitation were detected. When there was no cavitation, no phenomena were recorded.

Fig. 4 shows a sequence of images captured with the IR camera. A darker color on the images represents the colder region. An area of 6 × 6 mm is presented in the sequence. A time step between the images is 2 ms.
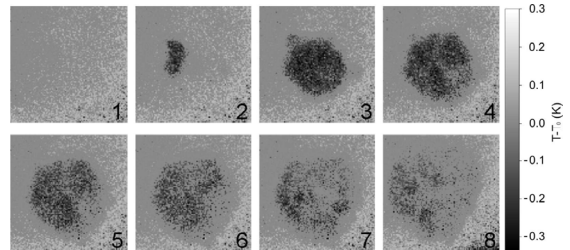

Fig. 4. *Sequence of images showing the evolution of the temperature field*

Spreading of a cold front, which resembles the shape of a cloud, is observed. The first frame shows the very beginning of the event, where the cloud has not been formed yet and only some small temperature deviations from the mean value, which might be related to the internal noise of the IR camera sensor, can be seen.

In the next time frame, a lower temperature region appears. Its shape is random at the beginning but evolves into circular form later on. Towards the end of the sequence, the cold front propagation velocity decreases and eventually stops. After that, the cold front shape deviates from the circular form and again becomes random.

The apparently warmer region that can be seen in the bottom right corner of all the images in Fig. 4, is a result of different emission coefficients of the cylinder that holds the silicon window and should not be interpreted as an actual temperature change.
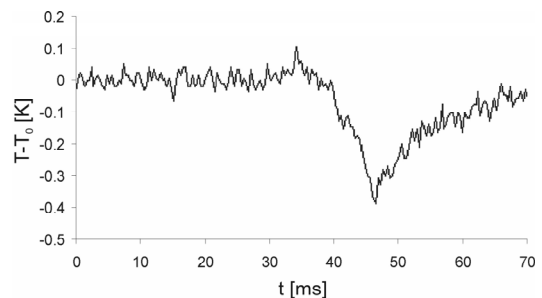

Fig. 5. *Evolution of temperature with time in a single point*

The temperature inside the cold front appears to be almost uniform. Small temperature

gradients, which appear randomly at the end of a sequence, can be related to mixing currents inside the vessel caused by cavitation.

Fig. 5 shows the temperature drop in a single point in the middle of the "cold cloud" from the sequence in Fig. 4. The evolution of the temperature is similar all over the cloud (apart from the shift in time) since its temperature is almost uniform.

Initially (at $t = 0$), the temperature is equal to the ambient temperature ($T-T_0 = 0$ K). At a certain point in time, a rapid drop in temperature can be seen. The temperature decreases from the initial temperature by approximately 0.35 K ($T-T_0 = -0.35$ K) in a period of about 10 ms. The temperature then exponentially rises (the heat flows from slightly warmer silicon glass). The last part of the exponential temperature evolution is gently sloping and is left out of the diagram for a clearer presentation of the central part of the drop. Eventually the temperature reaches the initial water temperature.

Small oscillations ($T-T_0 = \pm 0.02$ K) of temperature are the result of noise, which has not been filtered in order to preserve the complete signal.
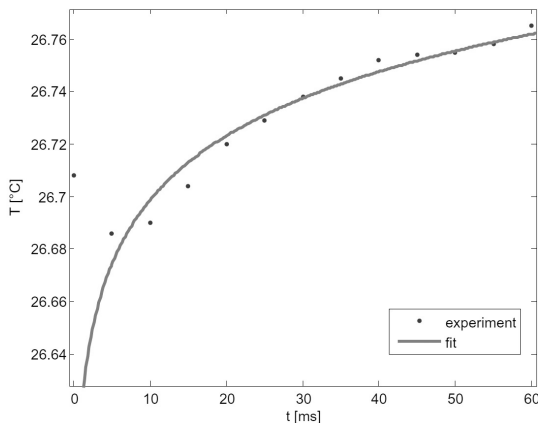

Fig. 6. *Evolution of the average temperature of the cloud and its exponential fit*

In Fig. 6 a time evolution of the average temperature of a cloud (dots) and an exponential approximation for a rising part are presented. This approximation seems suitable for a heat transfer after the initial temperature drop and the results show sound agreement with the experimental data (also mentioned above in Fig. 5). The first point which lies outside the proposed fit belongs to the part where the temperature is still decreasing and

which the fit does not cover. The rising temperature development is similar to the response of a system on a step change in a temperature. A step change could be represented by a phenomenon that caused the temperature drop, for which it should hold true that it is very short in time and has ceased after the temperature reached its minimum. Therefore, if the system answers a step change with the exponential response, then it must be described by a first-order differential equation. This is typical where heat conduction is prevalent. Thus, the detected temperature rise from the lowest temperature to the ambient (starting) temperature might be a result of the heat, going from the silicon glass plate back to the water touching it.

2.2 Kinematic Analysis

Raw images from the IR camera were processed in a way allowing the contours of the so-called clouds were extracted. They were approximated by circles and the average temperatures of the clouds were calculated (Fig. 7).
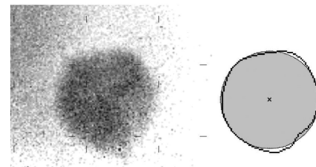

Fig. 7. *Raw image and processed image with detected edge and its approximation with a circle*

The edge of a cloud is representing a cold front, originating in microbubble generation caused by the splashing effect [16]. To find the edges, the Matlab edge function was used [17] and [18]. The edge function was used with the Canny method [19].

To study the phenomenon further, a propagation of the cold front was determined (Fig. 8).

The positions of the front correspond to the temperature fields in Fig. 4.

From the data of the front position in a specified time lapses, the propagation velocity could be determined. The mean velocity for the front movement in each time frame is based on a change of radius of the cloud, approximated by a circle. Velocities of the cloud spreading are presented as a function of time and the cloud radius (Fig. 9).
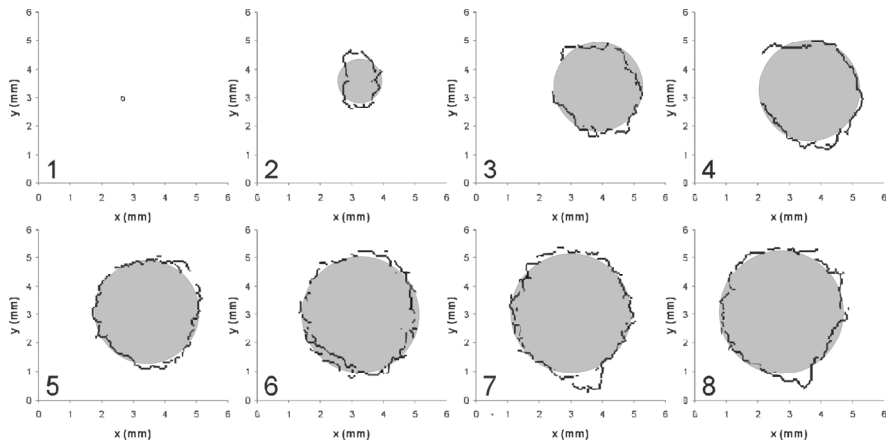
Fig. 8. *Propagation of the cold front, 1) initial state with almost no temperature effect, 2) first appearance of a cold cloud, 3–7) decelerated growth of the cloud, resulting in 8) a final size of a cold area*
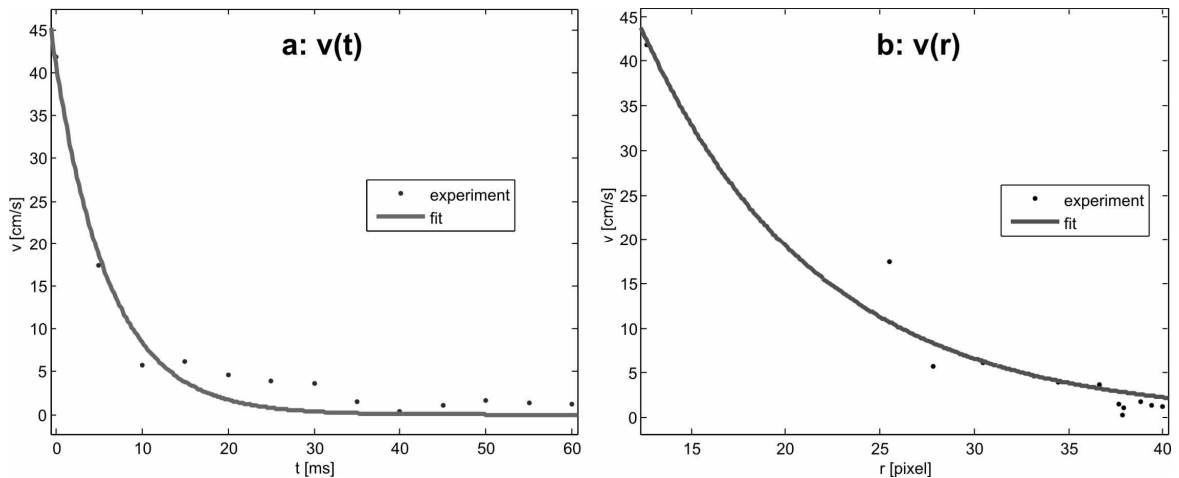

Fig. 9. *Velocity of the cold front propagation, a) as a function of time, b) as a function of radius*

The collapse, causing a splashing effect responsible for the observed local cooling, strongly depends on the initial size of the bubble and its distance from the solid wall [20, 21], therefore, for the fitting function, at least two coefficients are necessary. For this reason, an exponential function ae^{bx} was chosen without considering any other physical background.

However, data presented in Fig. 9 were fitted with the agreement $R^2 > 0.96$. Generally, sets of data (for an evolution of each single cloud) and appurtenant coefficients of fitting functions differ quite a lot, although the evolutions all share the same general shape.

A possible reason why, in some cases, the shape of the cloud differs from circular is the interaction between bubbles that appear close to one another or some not yet damped velocity field from previous collapses so that the microjet that forms during the collapse is no longer perpendicular to the solid wall.

3 CONCLUSIONS

Oscillations with ultrasound frequencies (42 kHz) were used to generate bubbles in a small tank. A silicon glass window was attached to the cylinder and partially submerged into water. Bubbles that imploded and grew in the vicinity of the window generated small temperature changes, which were recorded with a high speed thermocamera. Small but distinctive local temperature decreases in order of few 1/10 K with a duration in order of few 1/100 s were detected.

In this way, a new approach towards an experimental classification of cavitation on a local level by using infrared thermography was presented. The motivation was set by the lack of comparable methods whereas the aim was not to capture the extreme conditions that happen in the final stage of a collapse for which the method is still not fast enough.

Based on the obtained thermographic results a kinematic analysis was performed, where the expansion of the areas of temperature changes was investigated. The velocity of expansion was related to the characteristic area size as a function of two independent variables, indicating the effect of cavitation intensity and its distance from the wall.

The introduced thermographic method was applied on the ultrasound induced cavitation as an example of useful cavitation effects and as it is believed that the method can contribute to a better understanding of the cavitation phenomenon, this may lead to an improved performance of many practical applications where cavitation is present. In addition, as the water sensibility to cavitation thermal effects at room temperature is very weak [4] and [15], it may also be expected that the method will provide even better results in cases when hot water or other, e.g. cryogenic fluids, are used.

4 REFERENCES

[1] Franc, J.P., Michel, J.M. (2004). *Fundamentals of cavitation*. Dordrecht, The Netherlands.

[2] Fujikawa, S., Akamatsu, T. (1980). Effects of the non-equilibrium condensation of vapor on the pressure wave produced by the collapse of the bubble in a liquid. *Journal of Fluid Mechanics,* vol. 97, p. 481-512.

[3] Utturkar, Y., Wu, J., Wang, G., Shyy, W. (2005). Recent progress in modeling of cryogenic cavitation for liquid rocket propulsion. *Progress in Aerospace Sciences,* vol. 41, p. 558-608.

[4] Fruman, D.H., Reboud, J.L., Stutz, B. (1999). Estimation of thermal effects in cavitation of thermosensible liquids. *Int. Journal of Heat and Mass Transfer,* vol. 42, p. 3195-3204.

[5] Ishii, T., Murakami, M. (2003). Comparison of cavitating flows in He I and He II. *Cryogenics,* vol. 43, p. 507-514.

[6] Franc, J.P., Rebattet, C., Coulon, A. (2004). An experimental investigation of thermal effects in a cavitating inducer. *Journal of Fluids Engineering,* vol. 126, p. 716-723.

[7] Yoshida, Y., Kikuta, K., Watanabe, M., Hashimoto, T., Nagaura, K., Ohira, K. (2006). Thermodynamic effect on cavitation performances and cavitation instabilities in an inducer. *Proceeding of 6th International Symposium on Cavitation CAV2006*, Wageningen.

[8] Yoshida, Y., Sasao, Y., Okita, K., Hasegawa, S., Shimagaki, M., Nakamura, N., Ikohagi, T. (2006). Influence of thermodynamic effect on synchronous rotating cavitation. *Proceeding of 6th International Symposium on Cavitation CAV2006*, Wageningen.

[9] Mason, T.J., Lorimer, J.P. (2002). *Applied Sonochemistry*. Weinheim, Germany.

[10] Hale, G.M., Querry, M.R. (1973). Optical constant of water in the 200 nm to 200 μm wavelength region. *Appl. Opt.,* vol. 12, p. 555-563.

[11] Edmund Optics *http://www.edmundoptics.com* (2009), accesed on 2009-10-29.

[12] Benjamin, T.B., Ellis, A.T. (1966). The collapse of cavitation bubbles and the pressures thereby produced against solid boundaries. *Phil. Trans. Roy. Soc.*, vol. 260, p. 221-240.

[13] Plesset, M.S., Chapman, R.B. (1971). Collapse of an initially spherical vapor cavity in the neighbourhood of a solid boundary. *Journal of Fluid Mechanics,* vol. 47, no. 2, p. 283-290.

[14] Lauterborn, W., Bolle, H. (1975). Experimental investigations of cavitation-bubble collapse in the neighbourhood of a solid boundary. *J. of Fluid Mechanics,* vol. 72, no. 2, p. 391-399.

[15] Brennen, C.E. (1995). *Cavitation and bubble dynamics*, New York.

[16] Tong, R.P., Schiffers, W.P., Shaw, J.S., Blake, J.R., Emmony, D.C. (1999). The role of "splashing" in the collapse of the laser-generated cavity near a rigid boundary. *Journal of Fluid Mechanics,* vol. 380, p. 339-361.

[17] Lim, J.S. (1990). *Two-dimensional signal and image processing*. Englewood Cliffs, NJ, Prentice Hall, p. 478-488.

[18] Parker, J.R. (1997). *Algorithms for image processing and computer vision*. John Wiley & Sons, Inc., New York, p. 23-29.

[19] Canny, J. (1986). A computational approach to edge detection. *IEEE Transactions on Pattern Analysis and Machine Intelligence,* vol. 8, no. 6, p. 679-698.

[20] Reboud, J.L., Fortes-Patella, R., Archer, A. (1999). Analysis of damaged surfaces: part i: cavitation mark measurements by 3D laser profilometry. *Proceedings of the 3rd ASME / JSME Joint Fluids Engineering Conference*, San Francisco.

[21] Philipp, A., Lauterborn, W. (1998). Cavitation erosion by single laser-produced bubbles. *Journal of Fluid Mechanics,* vol. 361, p. 75-116.

Osterman, A. – Dular, M. – Hočevar, M. – Širok, B.